



## Research Paper

Macroporous carrier-free Sr-Ti catalyst for NO<sub>x</sub> storage and reduction

Virginia Alcalde-Santiago<sup>a</sup>, Arantxa Davó-Quiñonero<sup>a</sup>, Ion Such-Basáñez<sup>b</sup>, Dolores Lozano-Castelló<sup>a</sup>, Agustín Bueno-López<sup>a,\*</sup>

<sup>a</sup> Department of Inorganic Chemistry, University of Alicante, Carretera de San Vicente s/n. E03080, Alicante, Spain

<sup>b</sup> Technical Research Services (SSTI), University of Alicante, Carretera de San Vicente s/n. E03080, Alicante, Spain

## ARTICLE INFO

## Keywords:

NO<sub>x</sub>  
NSR  
LNT  
deNO<sub>x</sub>  
Macroporous  
Sr-Ti  
Mixed oxide  
Perovskite

## ABSTRACT

A novel concept is presented, consisting of a macroporous carrier-free catalyst. As a proof of concept, a novel Cu-containing Sr-Ti NSR catalyst with a macroporous network has been synthesized, and its maximum NO<sub>x</sub> storage capacity (1500  $\mu\text{molNO}_x/\text{g}_{\text{catalyst}}$ ) significantly surpasses that of conventional Pt/Ba/Al<sub>2</sub>O<sub>3</sub> formulations ( $\sim 600$ –800  $\mu\text{molNO}_x/\text{g}_{\text{catalyst}}$ ). This high NO<sub>x</sub> storage capacity is achieved because the active phases (mainly SrCO<sub>3</sub> and Cu-containing Sr-Ti perovskites, as deduced by XRD) are not diluted in an inert carrier, and this can be done because the macroporous structure obtained using a polymethylmethacrylate colloidal crystal template allows the access of gases to the particles bulk. *In situ* DRIFTS experiments showed that NO<sub>x</sub> were chemisorbed on the novel Cu-containing Sr-Ti macroporous catalyst as a mixture of nitrite and nitro species, and this suggests that several NO<sub>x</sub> chemisorption pathways are simultaneously taking place probably involving chemisorption of both NO and NO<sub>2</sub>. Additionally, this novel catalyst is totally selective towards N<sub>2</sub> formation as NO<sub>x</sub> reduction product, without traces of N<sub>2</sub>O nor NH<sub>3</sub>. CO<sub>2</sub> and H<sub>2</sub>O compete with NO<sub>x</sub> for being chemisorbed on the catalyst, and this hinders the utilization of this catalyst in real diesel exhausts. However, we believe that this new concept of macroporous carrier-free catalyst could be extended to other heterogeneous catalyzed reactions or materials to avoid the diluting effect of the catalyst support.

## 1. Introduction

Heterogeneous catalytic reactions are an important and complex class of chemical reactions where, usually, reactants and products are gases or liquids and the reaction takes place on the surface of a solid catalyst [1,2]. In these systems, the amount of active sites on the catalyst surface where the fluid molecules are chemisorbed and transformed plays a key role. In order to maximize the amount of active sites exposed to the fluid, the active phases of heterogeneous catalysts are often dispersed on a high-surface area solid carrier. This allows stabilizing small particles of the active compounds, improving their surface/bulk ratio. However, this presents the drawback that the active phases are diluted, and it would be desirable to design catalysts with appropriate solid state, surface, and morphological properties but avoiding the diluting effect of the support.

A particular application where dilution of the active phases presents great disadvantages is NO<sub>x</sub> storage and reduction (NSR). NSR is one of the most suitable technologies for NO<sub>x</sub> removal in diesel exhausts, which is a hot topic of ongoing research [3–6]. It operates in cycles where NO<sub>x</sub> are continuously chemisorbed on a catalyst that is periodically regenerated by feeding pulses of a reductant. Conventional

NSR catalysts, like Pt/Ba/Al<sub>2</sub>O<sub>3</sub> formulations, combine a NO<sub>x</sub> storage compound (typically an alkali compound) with a noble metal to accelerate NO oxidation to NO<sub>2</sub>. In this application, high NO<sub>x</sub> storage capacity is required, and dispersion and dilution of the active phases has a negative impact in NO<sub>x</sub> chemisorption.

To avoid dispersion of the active phases, a novel concept is introduced in this paper. It comprises the preparation of macroporous carrier-free NSR catalysts by using a colloidal crystal template, which allows the access of gases to the particles' bulk. The utilization of colloidal crystal templates has demonstrated to be a suitable synthetic route to obtain solid catalysts with a macroporous structure [7,8], therefore improving the diffusion of gases in heterogeneous catalytic reactions [9–15]. However, macroporous catalysts prepared with colloidal crystal templates have never been tested for NO<sub>x</sub> storage and reduction.

The catalyst prepared in this study is a copper-containing Sr-Ti mixed oxide, mainly consisting of an intimate mixture of SrCO<sub>3</sub> and Sr-Ti perovskites. This mixture of phases has been specially designed to combine the high NO<sub>x</sub> chemisorption capacity of the former phase with the NO oxidation capacity of the latter [16,17]. The design and synthesis of specific tailor-made mixed oxides able to perform complex

\* Corresponding author.

E-mail address: [agus@ua.es](mailto:agus@ua.es) (A. Bueno-López).

functions is one of the main topics of research in the field of heterogeneous catalysis, and strontium titanates are mixed oxides with relevant catalytic applications [18–23]. The storage and reduction of NOx has been reported on copper-containing  $\text{SrTiO}_3$  [20], this catalyst being also active to accelerate diesel soot combustion [21]. Doped strontium titanates have been also proposed as potential materials for anodes in solid-oxide fuel cell operating directly on hydrocarbon fuels, because of the resistance towards carbon formation [24], for photocatalytic production of  $\text{H}_2$  [25], and for propane [26] and methane [27] oxidation.

The goal of this study is to demonstrate the high NOx storage capacity of the macroporous carrier-free catalyst prepared, and that stored NOx can be properly reduced to  $\text{N}_2$ .

## 2. Experimental details

### 2.1. Catalysts preparation

As a proof of concept, three catalysts have been prepared and tested, which are referred to as SrTi-macro, SrTiCu-macro and SrTi-ref. The catalysts SrTi-macro and SrTi-ref have the same composition, but the former has been prepared by infiltration of the metal precursors in a polymethylmethacrylate (PMMA) colloidal crystal template, which is removed by calcination, while the latter has been obtained by calcination of a mixture of precursors. The catalyst SrTiCu-macro is similar to SrTi-macro but doped with copper.

Polymethylmethacrylate (PMMA) colloidal crystals were prepared by polymerisation in boiling aqueous solution of methylmethacrylate, methacrylic acid and divinylbenzene in 100:1:5 vol ratio. Potassium persulfate was used to initiate the polymerization, which was conducted for 75 min. After cooling, the colloidal crystals of PMMA spheres were conformed by centrifugation.

For preparation of SrTi-macro, 5 g of PMMA template was impregnated with a 1:1 water:ethanol solution of strontium nitrate (1.15 g of strontium nitrate per gram of PMMA). After drying, titanium tetraisopropoxide (0.48 g per gram of PMMA) diluted in 2-propanol was impregnated and the solid was dried at 80 °C. The Sr:Ti atomic ratio used was 3.2, that is, there is an excess of Sr with respect to that required to yield the  $\text{SrTiO}_3$  perovskite. The goal was to prepare a mixture of phases combining  $\text{SrCO}_3$  (with high NOx storage capacity) and  $\text{SrTiO}_3$  (with high NO oxidation capacity). This was confirmed by XRD and microFRX (see below). The catalyst referred to as SrTiCu-macro was prepared following the same procedure, but in this case, copper nitrate was impregnated into PMMA together with strontium nitrate (strontium nitrate:copper nitrate weight ratio 34.5). The impregnated PMMAs were calcined at 650 °C for 1 h (heating rate of 1 °C/min) and the temperature was increased afterwards at 10 °C/min up to 850 °C. The reference catalyst, (SrTi-ref) was prepared with the same composition than SrTi-macro but without PMMA template.

For comparison, a reference 1%Pt/10%Ba/Al<sub>2</sub>O<sub>3</sub> catalyst was also prepared. Ba(CH<sub>3</sub>COO)<sub>2</sub> was loaded on commercial  $\gamma$ -alumina (Alfa Aesar 99.97%) by wetness impregnation using a water solution to reach 10 wt.% Ba, and after drying at 80 °C overnight, the same procedure was repeated with Pt(NH<sub>3</sub>)<sub>4</sub>(NO<sub>3</sub>) for 1 wt.% Pt loading. Finally, the catalyst was dried at 100 °C for 4 h and calcined at 550 °C for 4 additional hours.

### 2.2. Catalysts characterization

SEM images were obtained in a JEOL microscope, model JSM-840.

The porous structure of the catalysts was studied by mercury intrusion porosimetry and  $\text{N}_2$  adsorption-desorption at −196 °C.  $\text{N}_2$  adsorption-desorption isotherms were obtained in an automatic volumetric system (Autosorb-6, Quantachrome) and data were evaluated by calculating BET surface areas. The catalysts were outgassed at 150 °C for 4 h before the  $\text{N}_2$  adsorption measurements.

Mercury porosimetry analysis was performed in a Poremaster 60 GT

(Quantachrome). This equipment is capable of intruding mercury up to 60000 psi reaching pores with diameters of 3.6 nm. All powdered samples were submitted to a prior outgassing treatment at 50 °C under vacuum (10 Torr) for 12 h. Samples were then analyzed in low pressure mode and high pressure mode consecutively. A contact angle ( $\theta$ ) of 140 °C and a value of mercury surface tension ( $\gamma$ ) of 0.48 J/m<sup>2</sup> were used. Intrusion pressure relates inversely to the pore diameter through the Washburn equation but has to be reminded that pore diameter obtained relates to the entrance of the pore while pore diameter through the channel may vary [28]. Mercury porosimetry of powder samples is complex due to the occurrence of interparticle and intraparticle intrusions as well as bed packing effects. Such effects are considered to occur up to a pressure of 50 psia, which corresponds to a pore diameter of 2133 nm. For the sake of clarity, interparticle filling region is not shown (diameter greater than 2100 nm). Also, intrusion in pores smaller than 10 nm is not shown, as most probably is affected by compressibility of the sample.

The nature of the different crystallographic phases present on the catalysts was studied by XRD, and the composition by Micro-FRX. Diffractograms were obtained in a Rigaku Miniflex II diffractometer, using CuK $\alpha$  radiation ( $\lambda = 0.15418$  nm), between 10 and 60° (2 $\theta$ ) with a step of 0.025°. Micro-XRF measurements were performed in an Orbis Micro-XRF Analyzer from EDAX. Areas of 300  $\mu\text{m}$  in diameter were analyzed and three different spots were measured and averaged to obtain the mean composition of each catalyst.

The reducibility of the catalysts was studied by  $\text{H}_2$ -TPR experiments, which were performed in a Micromeritics Pulse ChemiSorb 2705 device. 40 mg of catalyst were loaded on a tubular quartz reactor with 5 mm inner diameter coupled to a thermal conductivity detector. The heating rate was 10 °C/min from room temperature to 1000 °C and the gas flow was 40 ml/min with 5 vol.%  $\text{H}_2$  in Ar. A cold trap was placed before the TCD, consisting of a mixture of isopropyl alcohol and liquid nitrogen (temperature −89 °C).

### 2.3. NOx chemisorption and NSR experiments

NOx chemisorption-desorption experiments were performed in temperature ramp conditions in a fixed-bed reactor coupled to specific NDIR-UV gas analyzers for NO,  $\text{NO}_2$  and  $\text{O}_2$  monitoring (Fisher-Rosemount, models BINOS). A gas stream (500 ml/min; GHSV = 30000 h<sup>−1</sup>) with 500 ppm NO + 5%  $\text{O}_2$  in  $\text{N}_2$  was used, and the experiments consisted of heating the reactor from room temperature up to 800 °C at 10 °C/min. The catalysts were kept at room temperature under the reaction gas mixture for 15 min before heating, but chemisorption in these conditions was null for all catalysts.

*In situ* DRIFTS isothermal experiments were performed at 450 °C with catalysts SrTi-macro and SrTiCu-macro, to identify the nature of the chemisorbed NOx species. An infrared spectrometer Jasco, model FT/IR-4100, was used with a reaction cell that allows temperature and gas flow composition control. The cell was designed to allow the gas flow through the catalytic bed, consisting of 100 mg of undiluted catalyst. The temperature was increased up to 450 °C in inert gas (Ar), and after 30 min a background spectrum was recorded and subtracted from further spectra. Then, the inert gas was replaced by 100 ml/min of a gas stream with 500 ppm NO + 5%  $\text{O}_2$  in Ar and the chemisorbed species were monitored as a function of time.

Isothermal NOx storage and NSR experiments were carried out in a fixed-bed reactor coupled to a mass spectrometer Pfeiffer Vacuum (model OmniStar) running at 1 s frequency. The experiments were performed with 80 mg of the catalyst SrTiCu-macro diluted with 300 mg of SiC. The temperature was increased up to 450 °C in Ar flow, and then the inert gas was replaced by the reaction gas mixture (100 ml). The NOx chemisorption experiments were carried out with 500 ppm NO + 5%  $\text{O}_2$  in Ar. The NSR experiments were also performed with 500 ppm NO + 5%  $\text{O}_2$  in Ar and with 500 ppm NO + 5%  $\text{O}_2$  + 5%  $\text{CO}_2$  + 5%  $\text{H}_2\text{O}$  in Ar. All gases were added to the mixture

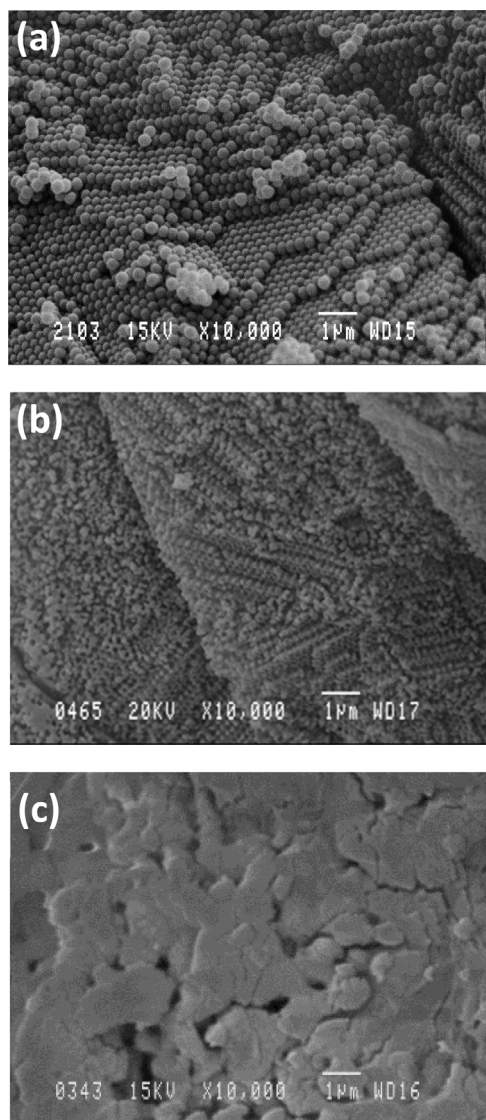


Fig. 1. SEM images of (a) PMMA template, (b) SrTi-macro and (c) SrTi-ref.

using mass flow controllers except  $\text{H}_2\text{O}$ , than was feed passing the gas mixture through a gas saturator. NSR experiments were carried out with  $\text{H}_2$  pulses using an injection valve with a 100  $\mu\text{l}$  loop that was

periodically filled with pure  $\text{H}_2$  at 10 psi.  $\text{H}_2$  was feed to the main stream at 2 min intervals.

### 3. Results and discussion

#### 3.1. Catalysts characterization by SEM, mercury porosimetry and $\text{N}_2$ adsorption

Fig. 1 shows images of the PMMA colloidal crystal template (Fig. 1a), SrTi-macro catalyst (Fig. 1b) and SrTi-ref catalyst (Fig. 1c). Monodisperse spheres of PMMA with about 200 nm diameter are observed in Fig. 1a, which are packed in regular planes forming the colloidal crystal. The catalyst prepared by infiltration into the PMMA template (Fig. 1b) shows the opposite morphology, with large spherical macropores arranged in the same way as the PMMA spheres. On the contrary, the reference catalyst (Fig. 1c), prepared without template, shows the agglomeration of large particles.

These important differences in the morphology of the catalysts prepared with and without PMMA template significantly affect the materials macroporosity, and in the end, the catalytic behavior of the solids. Pore size distributions determined by mercury intrusion porosimetry are included in Fig. 2, where the vertical line at a diameter of 50 nm indicates the pore size limit between mesopores and macropores according to the IUPAC recommendation [29]. Mercury intrusion (Fig. 2) shows that catalysts termed macro present little porosity in the mesopore range, most of their porosity being in the range of macropores. This confirms that PMMA templating is inducing the generation of macropores in materials SrTi-macro and SrTiCu-macro that are not present in the reference material SrTi-ref.

Fig. 3 shows the  $\text{N}_2$  adsorption-desorption isotherms at  $-196^\circ\text{C}$  of the prepared catalysts. Isotherms are non-reversible Type II isotherms with H3 hysteresis in the range of relative pressures ( $p/p_0$ ) between 0.8–1 [29]. No presence of pore-blocking artifacts at the end of the hysteresis loop is observed [28]. This fact can be important from the point of view of improving diffusion of gases in the catalytic systems. These features are representative of porous solids with no presence of micropores ( $< 2$  nm) or small mesopores (2–10 nm), a low contribution of larger mesopores (10–50 nm) and an important contribution of macropores arranged in some sort of 3D pore network, as indicated by the hysteresis loop.

Table 1 presents BET surface areas obtained from  $\text{N}_2$  adsorption isotherms at  $-196^\circ\text{C}$  and also mercury intrusion porosimetry areas. All surface areas are very low, which is consistent with the absence of micropores and small mesopores on the samples. PMMA-templated samples present slightly higher BET and Hg porosimetry areas than the

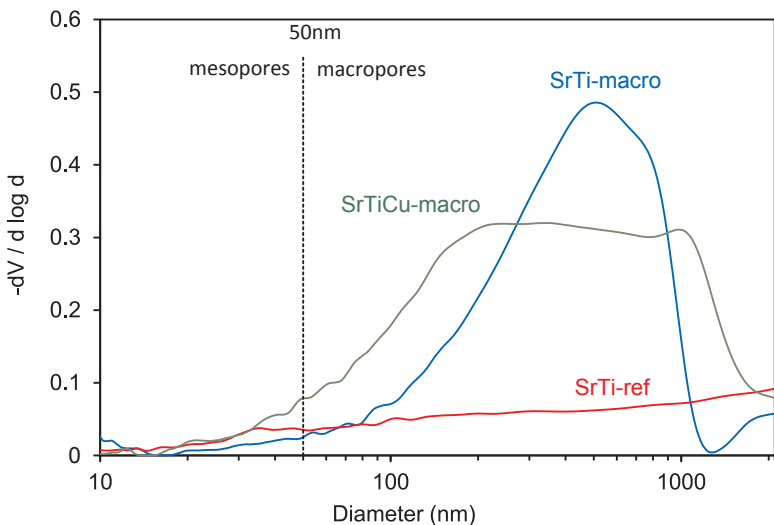
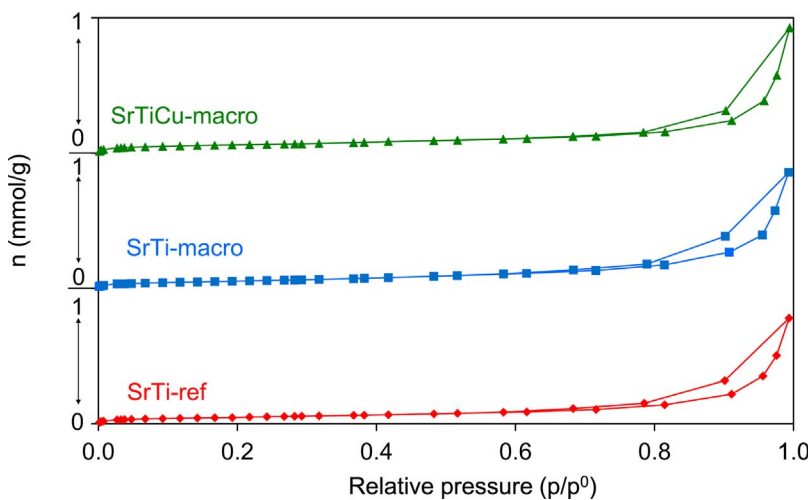


Fig. 2. Pore size distribution determined by mercury intrusion porosimetry.



**Table 1**  
BET specific surface areas and corrected Hg porosimetry surface areas

Catalyst	BET Surface area (m <sup>2</sup> /g)	Hg Surface area <sup>a</sup> (m <sup>2</sup> /g)
SrTiCu-macro	5	6
SrTi-macro	5	5
SrTi-ref	4	4

<sup>a</sup> Hg porosimetry areas have been corrected ruling out the effect of interparticle intrusion and compressibility effects.

non-templated sample, supporting the idea that template is inducing the generation of macroporosity. It is important to note that mercury intrusion porosimetry areas are expected to be slightly overestimated in some cases due to overlapping compressibility effects that are difficult to separate from pore intrusion phenomena.

### 3.2. Catalysts characterization by XRD and MicroFRX

Diffractograms of the catalysts are included in Fig. 4 and results of the MicroFRX analysis on Table 2, where it is observed that Sr is the

most abundant metal on all catalysts.

All diffractograms evidence the presence of several phases, including  $\text{TiO}_2$  (rutile),  $\text{SrCO}_3$ ,  $\text{Sr}_2\text{TiO}_4$  and  $\text{SrTiO}_3$ , and the main peaks of these phases have been labelled in Fig. 4. These species have also been detected by other authors for Sr-Ti mixed oxides calcined at temperatures similar to those used in this study [30]. The  $\text{SrTiO}_3$  perovskite phase is formed through the reaction of  $\text{TiO}_2$  with  $\text{SrO}$ , which first yields  $\text{Sr}_2\text{TiO}_4$  [31], and afterwards, by prolonged annealing in presence of  $\text{TiO}_2$ , would form the  $\text{SrTiO}_3$  perovskite phase. Therefore,  $\text{Sr}_2\text{TiO}_4$  phase is an intermediate in the formation reaction of  $\text{SrTiO}_3$  and this explains its modified-perovskite structure, which can be considered as a stacking of Sr-terminated  $\text{SrTiO}_3$  perovskite [001] slabs [32].

The rutile ( $TiO_2$ ) peak at  $27.0^\circ$  is absent in the copper-free catalysts and is quite small in the copper-containing one. This is consistent with the low amount of Ti with regard Sr detected by MicroFRX (Table 2). CuO peaks are not identified in the diffractogram of the catalyst SrTiCu-macro, which means that either copper cations are located in the  $Sr_2TiO_4$  and/or  $SrTiO_3$  perovskite structures, or segregated CuO, if present, is well dispersed and is not detected by XRD.

The crystal sizes of  $\text{Sr}_2\text{TiO}_4$  and  $\text{SrCO}_3$  have been determined with the Scherrer equation and the results, which are included in Table 2, are

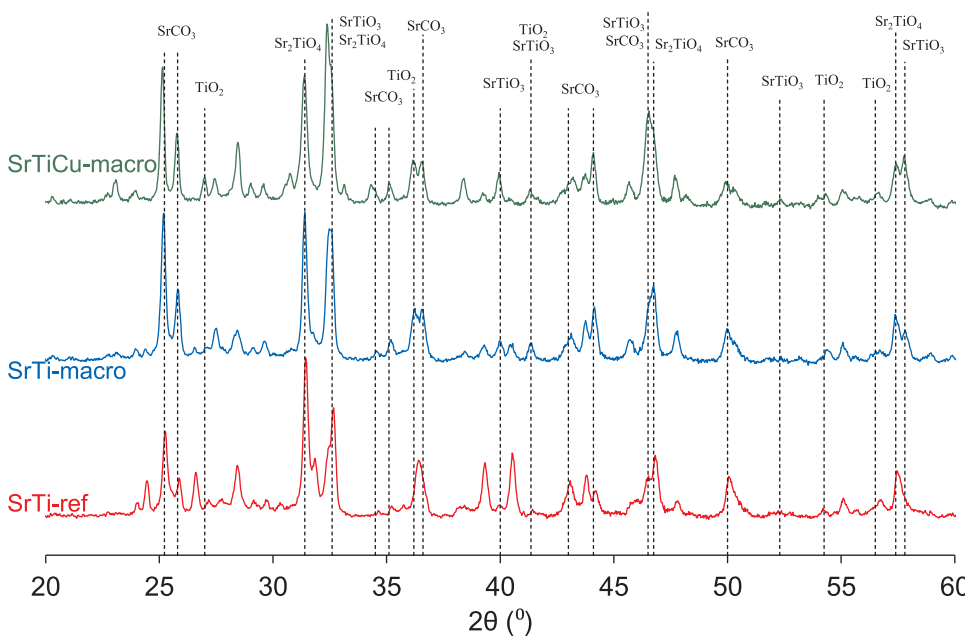


Fig. 4. X-Ray diffractograms of the catalysts.

**Table 2**

Micro-FRX characterization of the catalysts and crystal sizes determined with the Scherrer equation.

	Ti (at.%)	Cu (at.%)	Sr (at.%)	SrCO <sub>3</sub> (nm)	Sr <sub>2</sub> TiO <sub>4</sub> (nm)
				peak at 25.2°	peak at 31.4°
SrTiCu-macro	15.44 ± 1.45	2.01 ± 0.02	82.55 ± 1.46	43	29
SrTi-macro	13.22 ± 1.83	–	86.78 ± 1.83	39	36
SrTi-ref	13.59 ± 1.69	–	86.41 ± 1.69	42	33

quite similar for all catalysts suggesting that there are not important differences among them.

In conclusion, Micro-FRX and XRD characterization point out that, in spite of the complex composition of the catalysts, they mainly consist of SrCO<sub>3</sub> and the Sr-Ti perovskite-like structures Sr<sub>2</sub>TiO<sub>4</sub> and/or the SrTiO<sub>3</sub>. This combination of phases is very favorable for NO<sub>x</sub> removal by NSR technology, because it combines SrCO<sub>3</sub>, which has high NO<sub>x</sub> storage capacity, with copper-containing Sr-Ti perovskites, which accelerate NO oxidation to NO<sub>2</sub>, both being intimately mixed.

### 3.3. Catalysts characterization by temperature programmed reduction with H<sub>2</sub> (H<sub>2</sub>-TPR)

The reduction profiles obtained in H<sub>2</sub>-TPR experiments are included in Fig. 5, where all catalysts show a high temperature reduction peak around 850 °C that must be attributed to bulk reduction of the Sr-Ti mixed oxides. The areas under these peaks evidence that the bulk reduction of catalysts with macroporous structure is improved with regard to that of the reference catalysts prepared without PMMA template. Probably, the macroporous structure improves the diffusion of H<sub>2</sub> into the solid allowing a more efficient reduction.

The copper-containing catalyst (SrTiCu-macro) is more reducible than the copper-free counterpart (SrTi-macro), as expected due to the reduction of copper cations and to the catalytic effect of copper on the reduction of the SrTi perovskite structures. In addition, the copper-containing catalyst shows a lower temperature peak (200–500 °C) that could be tentatively assigned to the reduction of segregated copper oxide, to the reduction of surface Sr-Ti perovskites catalyzed by metal copper and/or to the reduction or release of species like carbonates or hydroxyls.

These H<sub>2</sub>-TPR experiments allow concluding that the macroporous structure favors bulk reduction of the mixed oxides with regard to non-macroporous counterparts, and the improved accessibility of gases to the particles bulk would also explain the enhanced chemisorption of NO<sub>x</sub> and the extremely high NO<sub>x</sub> storage capacity of the SrTiCu-macro

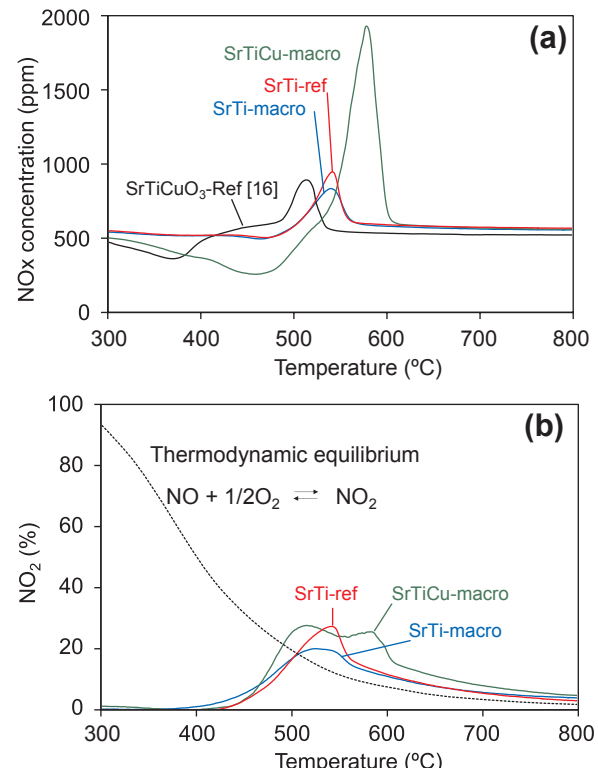


Fig. 6. Temperature programmed reactions performed in a gas mixture with 500 ppm NO<sub>x</sub> + 5% O<sub>2</sub>. (a) NO<sub>x</sub> profiles and (b) NO<sub>2</sub> percentages. The catalyst referred to as SrTiCuO<sub>3</sub>-Ref [16], which is the best strontium titanate we have tested so far for NO<sub>x</sub> storage [16] has been included together with those prepared in the current study for comparison.

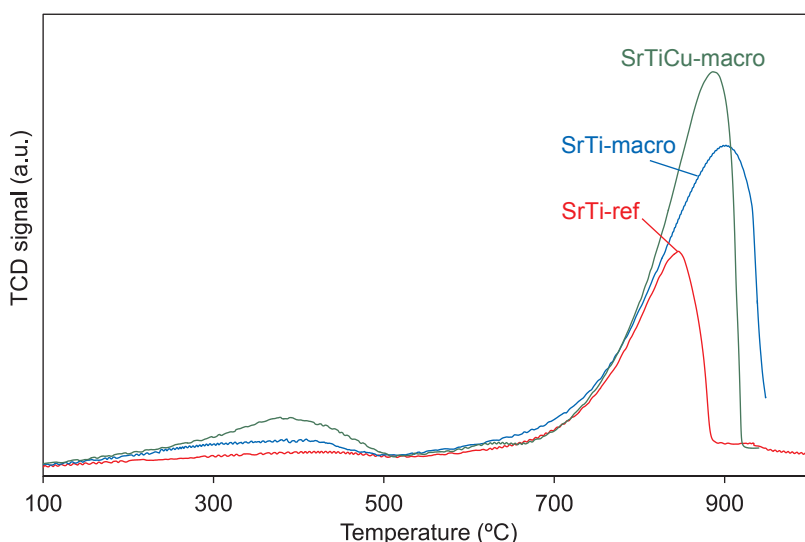


Fig. 5. Temperature programmed reductions with H<sub>2</sub>.

catalyst, as shown below.

### 3.4. NO<sub>x</sub> chemisorption

The chemisorption and desorption of NO<sub>x</sub> on the catalysts was studied by Temperature Programmed Reactions in a fixed-bed reactor. Fig. 6a shows the NO<sub>x</sub> profiles as a function of temperature and Fig. 6b the corresponding NO<sub>2</sub> profiles. All catalysts chemisorb NO<sub>x</sub> above 300 °C approximately, and the stored NO<sub>x</sub> decompose at higher temperature closing the mass balances. The amount of NO<sub>x</sub> chemisorbed and released depends on the catalyst composition and structure. For comparison purposes, the NO<sub>x</sub> chemisorption-desorption profile obtained with the catalyst referred to as SrTiCuO<sub>3</sub>-Ref [16] has been also included in Fig. 6a. This is the best copper-containing strontium titanate we had tested so far for NO<sub>x</sub> storage, and details about its preparation (sol-gel method; 850 °C calcination), characterization, NO<sub>x</sub> chemisorption and NSR performance were previously reported elsewhere [16,17]. The macroporous copper-containing catalyst (SrTiCu-macro) significantly outperforms its behavior, as deduced from the areas of the chemisorption and desorption peaks. This enhanced chemisorption of NO<sub>x</sub> on the macroporous catalyst SrTiCu-macro with respect to SrTiCuO<sub>3</sub>-Ref [16] is assigned to a better accessibility of NO<sub>x</sub> into the particles' bulk.

On the other hand, the copper-containing catalyst (SrTiCu-macro) chemisorbs more NO<sub>x</sub> than the copper-free counterpart (SrTi-macro), as expected. This improved chemisorption upon copper loading can be related to the improved NO oxidation capacity, as it has been previously reported [24]. It is known that copper accelerates the oxidation of NO, and that NO<sub>2</sub> is chemisorbed much better than NO. Nevertheless, Fig. 6b does not show higher NO<sub>2</sub> production by the copper containing catalyst, and this is because the NO<sub>2</sub> yielded is not released, but it remains chemisorbed on the catalyst. All NO<sub>2</sub> profiles of Fig. 6b are quite similar, increasing above 400 °C approximately and decreasing after the maxima are attained. Note that the release of NO<sub>2</sub> (Fig. 6b) starts at temperatures well above the onset of NO<sub>x</sub> chemisorption temperature (Fig. 6a), and this is consistent with the hypothesis about NO<sub>2</sub> chemisorption. Worth to mention is the fact that the NO<sub>2</sub> profiles exceed the equilibrium concentration at the maxima, because part of the NO<sub>2</sub> released at the maxima come from the decomposition of the NO<sub>x</sub> species stored at lower temperatures, and not only from the catalytic oxidation of NO taking place at that temperature [33].

The maximum NO<sub>x</sub> storage capacity of the catalyst SrTiCu-macro catalyst was measured under isothermal conditions at 450 °C, which is the temperature of the maximum in NO<sub>x</sub> chemisorption observed in Fig. 6. This NO<sub>x</sub> storage capacity is included in Table 3 together with values of reference materials reported in the literature. For each catalyst, and when indicated in the original source, the data included in Table 3 corresponds to the temperature of maximum NO<sub>x</sub> storage

**Table 3**  
Amount of NO<sub>x</sub> stored on selected catalysts.

Catalyst	NO <sub>x</sub> stored (μmolNO <sub>x</sub> / g <sub>catalyst</sub> )	Temperature (°C)	Reference
SrTiCu-macro	1500	450	This work
5%Cu/(BaO/BaCO <sub>3</sub> )	1204	400	[37]
0.24%Pt-8%Mn-20%K/ Al <sub>2</sub> O <sub>3</sub> -CeO <sub>2</sub>	980	400	[38]
0.8%Pt-23%Ba/Al <sub>2</sub> O <sub>3</sub>	800	350	[39]
1%Pt-10%Ba/Al <sub>2</sub> O <sub>3</sub>	714	400	[34]
1%Pt-20%Ba/Al <sub>2</sub> O <sub>3</sub>	581	300	[40]
Pt-Ru/Ba/ Al <sub>2</sub> O <sub>3</sub> -Ce <sub>0.33</sub> Zr <sub>0.67</sub> O <sub>2</sub>	446	300	[41]
1%Pt/10%Ba/Al <sub>2</sub> O <sub>3</sub>	271	400	This work
SrTi(Cu)O <sub>3</sub>	244	300	[16,17]
5%Cu/CeO <sub>2</sub>	168	400	[38]

capacity. NO<sub>x</sub> storage capacity was also measured in this study for a reference catalyst with composition 1%Pt/10%Ba/Al<sub>2</sub>O<sub>3</sub> catalyst.

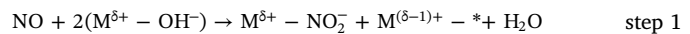
Data on Table 3 show that the NO<sub>x</sub> storage capacity of the macroporous carrier-free catalyst SrTiCu-macro prepared with the colloidal crystal template is very high and outperforms the storage capacity of other reported catalysts, including those containing noble metals. It amounts to 1500 μmolNO<sub>x</sub>/g<sub>catalyst</sub>, which is twice, for instance, that stored by a reference 1%Pt-10% Ba/Al<sub>2</sub>O<sub>3</sub> catalyst [34] and also much higher to that chemisorbed by our reference 1%Pt/10%Ba/Al<sub>2</sub>O<sub>3</sub> catalyst (271 μmolNO<sub>x</sub>/g<sub>catalyst</sub>) measured in this study in the same experimental set up than SrTiCu-macro.

This high NO<sub>x</sub> storage capacity of SrTiCu-macro can be explained considering that the active species for NO oxidation and NO<sub>x</sub> storage are not dispersed (and diluted) on Al<sub>2</sub>O<sub>3</sub>, as it must be done with conventional barium-based catalysts to obtain good dispersion. In our case, the macroporous structure allows utilization of the active species of the catalyst (mainly copper-containing strontium titanates and strontium carbonate, as shown in the XRD analysis) without dilution in an inert carrier.

The nature of the chemisorbed NO<sub>x</sub> species formed on the catalysts was studied by in situ DRIFTS experiments, and time-resolved spectra obtained with SrTi-macro and SrTiCu-macro under 500 ppm NO + 5% O<sub>2</sub> gas flow are included in Fig. 7a and b, respectively.

The most relevant peaks of the chemisorbed NO<sub>x</sub> species appear in the 1700–1000 cm<sup>-1</sup> range. The copper-free catalyst (Fig. 7a) shows a single peak at 1260 cm<sup>-1</sup> that grows with time and that can be assigned to the formation of chemisorbed nitrites, probably in bridge configuration [35]. On the contrary, the copper-containing catalyst (Fig. 7b) shows two peaks, the one assigned to nitrites at 1260 cm<sup>-1</sup> and another one at 1355 cm<sup>-1</sup> that can be related to the formation of nitro groups [35]. The difference between nitrite and nitro groups is that, in the former, nitrogen oxide is attached to the solid surface by an oxygen atom while in the latter is attached by the nitrogen atom.

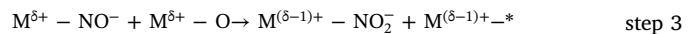
Adsorbed nitrite/nitro species can be formed upon NO chemisorption on hydroxyl groups [35]:



where “M<sup>δ+</sup> – OH<sup>-</sup>” are hydroxyl groups attached to metal cations that can accomplish the redox cycle M<sup>δ+</sup>/M<sup>(δ-1)+</sup>, that is, Ti and/or Cu cations in our catalysts. The chemisorption of NO on such hydroxyls yields an adsorbed nitrite/nitro “M<sup>δ+</sup> – NO<sub>2</sub><sup>-</sup>” and leaves an oxygen vacancy “M<sup>(δ-1)+</sup> – \*” on the catalysts that must be filled in a further step with oxygen from molecular oxygen or with NO, yielding nitrosyl anions “M<sup>δ+</sup> – NO<sup>-</sup>” as follows



Nitrosyl anions are hardly identified by infrared spectroscopy because their bands overlap with those of nitrites but, in oxidizing conditions, can be formed as transient species in the formation of nitrites/nitro:



The formation of nitrites/nitro throughout step 2 + step 3 requires the participation of easily reducible cations that must be able to provide oxygen for nitrosyl oxidation (step 3). This mechanism is expected to be enhanced by the presence of copper, since cations of this element accomplish redox cycles much more easily than those of Ti.

An additional reaction pathway for nitrite/nitro formation would involve the catalytic oxidation of NO to NO<sub>2</sub>, and the chemisorption of NO<sub>2</sub> on partially reduced cations (step 4):



The mechanism involving step 4 is also more probable to occur on the copper-containing catalyst (SrTiCu-macro) than on the copper-free one (SrTi-macro), because copper improves the oxidation capacity of the catalyst and this is necessary for NO<sub>2</sub> production [36].

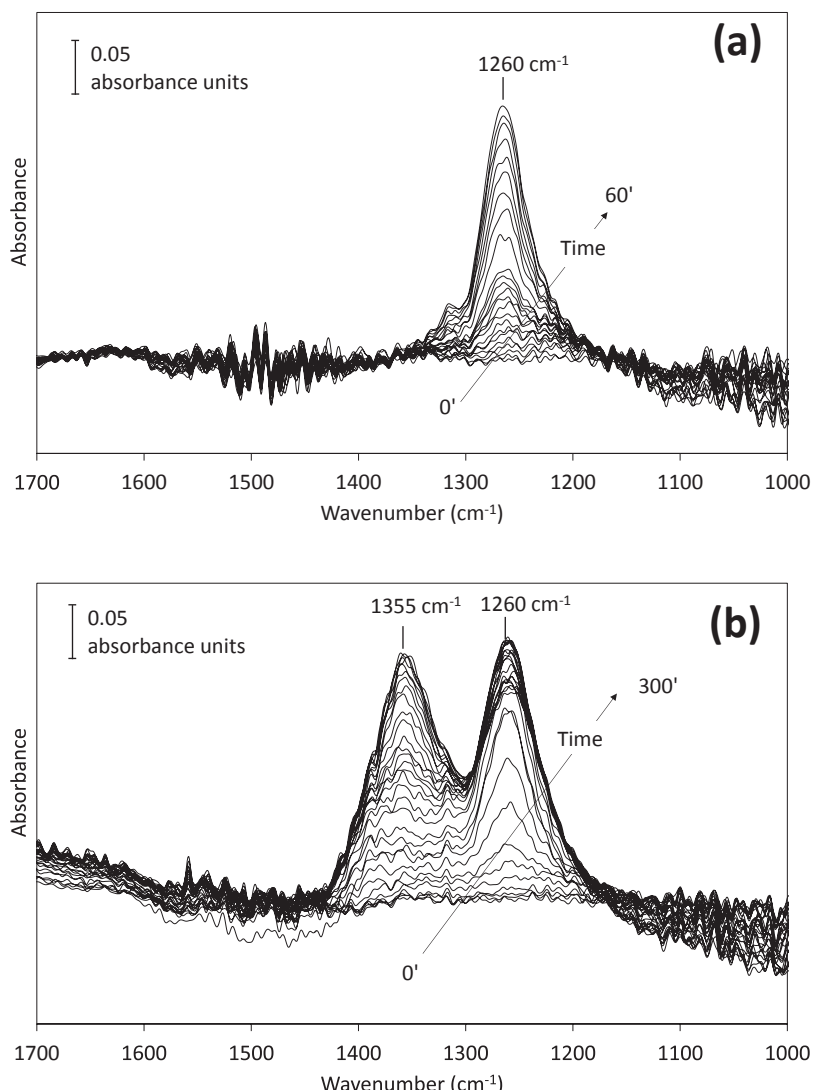


**Fig. 7.** *in situ* DRIFT spectra recorded at 450 °C under 500 ppm NO<sub>x</sub> + 5% O<sub>2</sub> stream in the 1700–1000 cm<sup>-1</sup> range for nitrogen surface species monitoring. (a) SrTi-macro catalyst and (b) SrTiCu-macro catalyst.

The simultaneous formation of nitrite and nitro groups on the SrTiCu-macro catalyst (Fig. 7b) suggests NO<sub>x</sub> chemisorption by different mechanisms and/or the presence of chemisorption sites of different nature, while the only formation of nitrites on SrTi-macro catalyst (Fig. 7b) indicates that the NO<sub>x</sub> chemisorption mechanism is simpler in this case. One hypothesis could be that NO chemisorption on the copper-free catalyst (SrTi-macro) only involves step 1 while NO<sub>x</sub> chemisorption on SrTiCu-macro additionally involves steps 2–4 together with step 1.

As a summary of the NO<sub>x</sub> chemisorption experiments and of the DRIFTS experiments, it is concluded that the SrTi catalysts chemisorb NO<sub>x</sub> above 300 °C approximately. Copper improves the NO<sub>x</sub> chemisorption capacity of the Sr-Ti catalyst and modifies the NO<sub>x</sub> chemisorption mechanism, involving several simultaneous chemisorption pathways and/or creating chemisorption sites of different nature. The macroporous structure of the catalyst drastically improves the NO<sub>x</sub> chemisorption capacity with regard to conventional-shaped catalysts.

### 3.5. NSR experiments

NSR experiments were carried out at 450 °C with SrTiCu-macro, and the NO<sub>x</sub> profile is shown in Fig. 8a. During the NSR cycles performed with NO<sub>x</sub> + O<sub>2</sub> in Ar, the chemisorption of NO<sub>x</sub> on the catalyst decreased NO<sub>x</sub> concentration from 500 ppm in the inlet gas to 200 ppm, keeping the removal of NO<sub>x</sub> constant for consecutive NSR cycles. This

evidences an appropriate balance between the amounts of NO<sub>x</sub> chemisorbed and reduced, and confirms that SrTiCu-macro behaves properly as NSR catalyst under these experimental conditions. After 30 min, CO<sub>2</sub> and H<sub>2</sub>O was included in the gas mixture and NO<sub>x</sub> concentration increased drastically, even above the concentration in the inlet gas. This indicates that the NO<sub>x</sub> species chemisorbed on the catalyst in the absence of CO<sub>2</sub> and H<sub>2</sub>O get unstable and are released in the presence of these species. This is attributed to the competition of CO<sub>2</sub>, H<sub>2</sub>O and NO<sub>x</sub> for the chemisorption sites of the catalyst. Note that the concentrations of CO<sub>2</sub> and H<sub>2</sub>O in the inlet gas (5%) are much higher to that of NO<sub>x</sub> (500 ppm). This is confirmed in Fig. 8b, where the CO<sub>2</sub> profile (m/z 44) is shown. It is observed that the m/z 44 signal does not increase rapidly once CO<sub>2</sub> is included in the reaction gas mixture, but raises smoothly because CO<sub>2</sub> is being chemisorbed on the catalyst. The same behavior is expected for H<sub>2</sub>O, but in this case was not possible to follow the H<sub>2</sub>O profile because a cold trap at –89 °C was located after the reactor to protect the mass spectrometer from the high H<sub>2</sub>O concentration.

Finally, the products selectivity was analyzed for NSR experiments performed under NO<sub>x</sub> + O<sub>2</sub> in Ar, and a representative NSR cycle is shown in Fig. 9, including the profiles of the potential NO<sub>x</sub> reduction products (m/z 28 (N<sub>2</sub>), m/z 44 (N<sub>2</sub>O) and m/z 17 (NH<sub>3</sub>)). Only a N<sub>2</sub> peak is observed, and this is the desired product while N<sub>2</sub>O or NH<sub>3</sub> undesired byproducts. These results confirm the high selectivity of the catalyst SrTiCu-macro towards the desired reduction product and the

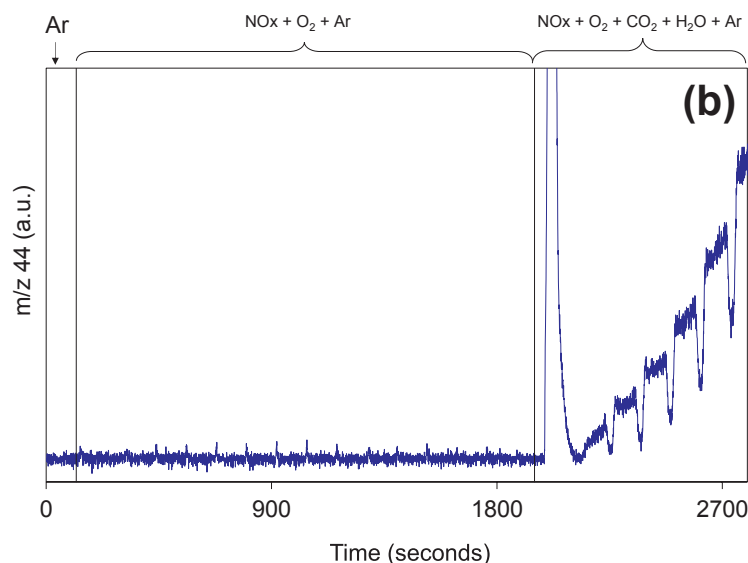
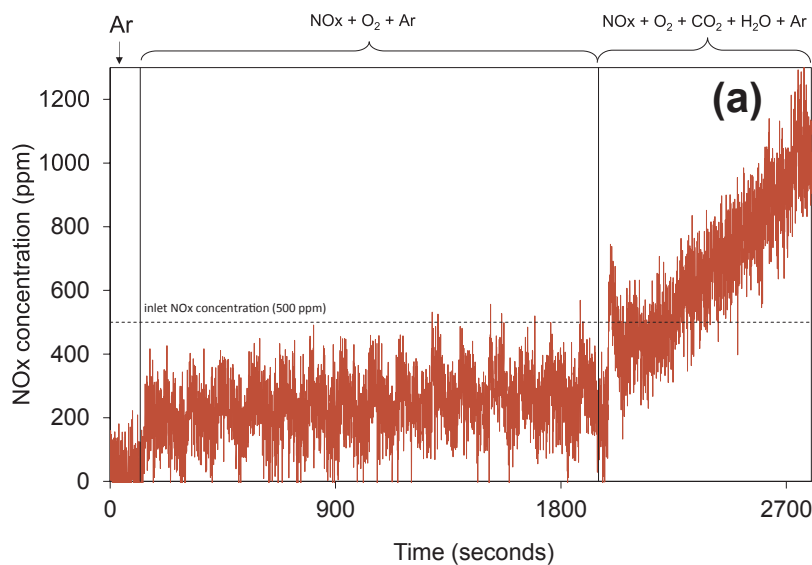


**Fig. 8.** NSR experiments performed with the catalyst SrTiCu-macro at 450 °C under 500 ppm NO + 5% O<sub>2</sub> in the absence and presence of 5% CO<sub>2</sub> and 5% H<sub>2</sub>O and with H<sub>2</sub> pulses. (a) NOx concentration and (b) m/z 44 signal (corresponding to CO<sub>2</sub> and/or N<sub>2</sub>O).

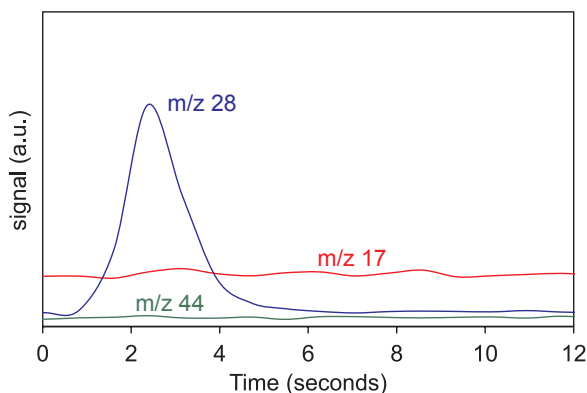


**Fig. 9.** Detail of the NOx reduction products ( $m/z$  28 N<sub>2</sub>,  $m/z$  44 N<sub>2</sub>O and  $m/z$  17 NH<sub>3</sub>) during a selected H<sub>2</sub> pulse performed in NSR cycles with the catalyst SrTiCu-macro at 450 °C under 500 ppm NOx + 5% O<sub>2</sub> in Ar.

absence of byproducts.

In conclusion, these experiments evidence that the catalyst SrTiCu-macro behaves properly as NSR catalyst in the absence of CO<sub>2</sub> and H<sub>2</sub>O, but not in the presence of these gases. This is a problem for the utilization of this catalyst in a real diesel exhaust. However, although only a

NSR catalyst has been tested as a case study, we believe that the concept of carrier-free macroporous catalyst can be extended to other heterogeneous catalytic reactions and also to other materials.

#### 4. Conclusions

In summary, it has been demonstrated that the synthesis of macroporous carrier-free catalysts is a successful way to obtain catalysts with very high NOx storage capacity. As a proof of concept, a macroporous carrier-free copper-containing Sr-Ti catalyst has been prepared with a colloidal crystal template (SrTiCu-macro). This catalyst is able to chemisorb NOx amounts even higher than those attained by noble metal catalysts. NOx are chemisorbed on SrTiCu-macro as a mixture of nitrite and nitro species, and this suggests that several NOx chemisorption pathways are simultaneously taking place probably involving chemisorption of both NO and NO<sub>2</sub>, and/or that the catalyst has chemisorption sites of different nature.

The stored NOx are conveniently reduced by H<sub>2</sub> with total selectivity towards N<sub>2</sub> formation.

CO<sub>2</sub> and H<sub>2</sub>O compete with NOx for the chemisorption sites on the SrTiCu-macro catalyst, and this is a limitation for the utilization of this material as NSR catalyst under real conditions of diesel engine exhaust.

## Acknowledgment

Authors thank the financial support from Generalitat Valenciana (Project PROMETEOII/2014/010), Spanish Ministry of Economy and Competitiveness (Projects MAT2014-61992-EXP and CTQ2015-67597-C2-2-R), Spanish Ministry of Education, Culture and Sports (grant FPU14/01178) and EU (FEDER funding).

## References

- [1] I. Chorkendorff, J.W. Niemantsverdriet, *Concepts of Modern Catalysis and Kinetics*, Wiley-VCH, Weinheim (Germany), 2007.
- [2] R. Schlögl, Heterogeneous catalysis, *Angew. Chem. Int. Ed.* 54 (2015) 3465–3520.
- [3] G. Liu, P.-X. Gao, A review of nox storage/reduction catalysts: mechanism, materials and degradation studies, *Catal. Sci. Technol.* 1 (2011) 552–568.
- [4] G. I. Whiteman, H. Hostet, Vehicle emissions: volkswagen and the road to Paris, *Nature* 527 (2015) 38.
- [5] J.P. Breen, C. Rioche, R. Burch, C. Hardacre, F.C. Meunier, Identifying critical factors in the regeneration of nox-trap materials under realistic conditions using fast transient techniques, *Appl. Catal. B* 72 (2007) 178–186.
- [6] J.P. Breen, R. Burch, C. Fontaine-Gautrelet, C. Hardacre, C. Rioche, Insight into the key aspects of the regeneration process in the NOx storage reduction (NSR) reaction probed using fast transient kinetics coupled with isotopically labelled  $^{18}\text{NO}$  over Pt and Rh-containing Ba/Al<sub>2</sub>O<sub>3</sub> catalysts, *Appl. Catal. B* 81 (2008) 150–159.
- [7] J.-P. Daquin, J. Dhainaut, D. Duprez, S. Royer, A.F. Lee, K. Wilson, An efficient route to highly organized, tunable macroporous-mesoporous alumina, *J. Am. Chem. Soc.* 131 (2009) 12896–12897.
- [8] W. Si, Y. Wang, Y. Peng, J. Li, Selective dissolution of A-site cations in ABO<sub>3</sub> perovskites: a new path to high-performance catalysts, *Angew. Chem. Int. Ed.* 54 (2015) 7954–7957.
- [9] Y. Wei, Z. Zhao, J. Liu, C. Xu, G. Jiang, A. Duan, Design and synthesis of 3D ordered macroporous CeO<sub>2</sub>-supported Pt@CeO<sub>2</sub>-<sub>8</sub> core-shell nanoparticle materials for enhanced catalytic activity of soot oxidation, *Small* 9 (2013) 3957–3963.
- [10] Y. Zhang, H. Liang, X.Y. Gao, Y. Liu, Three-dimensionally ordered macro-porous CuO–CeO<sub>2</sub> used for preferential oxidation of carbon monoxide in hydrogen-rich gases, *Catal. Commun.* 10 (2009) 1432–1436.
- [11] J. Zhang, Y. Jin, C. Li, Y. Shen, L. Han, Z. Hu, X. Di, Z. Liu, Creation of three-dimensionally ordered macroporous Au/CeO<sub>2</sub> catalysts with controlled pore sizes and their enhanced catalytic performance for formaldehyde oxidation, *Appl. Catal. B* 91 (2009) 11–20.
- [12] G. Zhang, Z. Zhao, J. Xu, J. Zheng, J. Liu, G. Jiang, A. Duan, H. He, Comparative study on the preparation, characterization and catalytic performances of 3dom ce-based materials for the combustion of diesel soot, *Appl. Catal. B* 107 (2011) 302–315.
- [13] G. Zhang, Z. Zhao, J. Liu, G. Jiang, A. Duan, J. Zheng, S. Chen, R. Zhou, Three dimensionally ordered macroporous Ce<sub>1-x</sub>Zr<sub>x</sub>O<sub>2</sub> solid solutions for diesel soot combustion, *Chem. Commun.* 46 (2010) 457–459.
- [14] Y. Wei, J. Liu, Z. Zhao, Y. Chen, C. Xu, A. Duan, G. Jiang, H. He, Highly active catalysts of gold nanoparticles supported on three-dimensionally ordered macro-porous LaFeO<sub>3</sub> for soot oxidation, *Angew. Chem. Int. Ed.* 50 (2011) 2326–2329.
- [15] K. Ji, H. Dai, J. Deng, X. Li, Y. Wang, B. Gaoa, G. Baia, C. Tong Au, A comparative study of bulk and 3DOM-structured Co<sub>3</sub>O<sub>4</sub>, Eu<sub>0.6</sub>Sr<sub>0.4</sub>FeO<sub>3</sub>, and Co<sub>3</sub>O<sub>4</sub>/Eu<sub>0.6</sub>Sr<sub>0.4</sub>FeO<sub>3</sub> preparation, characterization, and catalytic activities for toluene combustion, *Appl. Catal. A* 447–448 (2012) 41–48.
- [16] F.E. López-Suárez, M.J. Illán-Gómez, A. Bueno-López, J.A. Anderson, NOx storage and reduction on a SrTiCuO<sub>3</sub> perovskite catalyst studied by operando DRIFTS, *Appl. Catal. B* 104 (2011) 261–267.
- [17] F.E. López-Suárez, S. Parres-Escalp, A. Bueno-López, M.J. Illán-Gómez, B. Ura, J. Trawczynski, Role of surface and lattice copper species in copper-containing (Mg/Sr)TiO<sub>3</sub> perovskite catalysts for soot combustion, *Appl. Catal. B* 93 (2009) 82–89.
- [18] A. Kumar, P.G. Santangelo, N.S. Lewis, Electrolysis of water at SrTiO<sub>3</sub> photoelectrodes: distinguishing between the statistical and stochastic formalisms for electron-tranfer processes in fuel-forming photoelectrochemical systems, *J. Phys. Chem.* 96 (1992) 834–842.
- [19] K. Iwashina, A. Kudo, Rh-doped SrTiO<sub>3</sub> photocatalyst electrode showing cathodic photocurrent for water splitting under visible-light irradiation, *J. Am. Chem. Soc.* 133 (2011) 13272–13275.
- [20] J.W. Fergus, Perovskite oxides for semiconductor-based gas sensors, *Sens. Actuators B* 123 (2007) 1169–1179.
- [21] A. Chongtertoonskul, J.W. Schwank, S. Chavadej, Effects of oxide supports on ethylene epoxidation activity over Ag-based catalysts, *J. Molec. Catal. A* 358 (2012) 58–66.
- [22] H. Wang, J. Lu, C.L. Marshall, J.W. Elam, J.T. Miller, H. Liu, J.A. Enterkin, R.M. Kennedy, P.C. Stair, K.R. Poeppelmeier, L.D. Marks, In situ XANES study of methanol decomposition and partial oxidation to syn-gas over supported Pt catalyst on SrTiO<sub>3</sub> nanocubes, *Catal. Today* 237 (2014) 71–79.
- [23] B. Lertpanyapornchai, C. Ngamcharussrivichai, Mesostructured Sr and Ti mixed oxides as heterogeneous base catalysts for transesterification of palm kernel oil with methanol, *Chem. Eng. J.* 264 (2015) 789–796.
- [24] A. Atkinson, S. Barnett, R.J. Gorte, J.T.S. Irvine, A.J. Mcevoy, M. Mogensen, S.C. Singhal, J. Vohs, Advanced anodes for high-temperature fuel cells, *Nature Mat.* 3 (2004) 17–27.
- [25] K. Yu, C. Zhang, Y. Chang, Y. Feng, Z. Yang, T. Yang, L.-L. Lou, S. Liu, Novel three-dimensionally ordered macroporous SrTiO<sub>3</sub> photocatalysts with remarkably enhanced hydrogen production performance, *Appl. Catal. B* 200 (2017) 514–520.
- [26] J.A. Enterkin, W. Setthapun, J.W. Elam, S.T. Christensen, F.A. Rabuffetti, L.D. Marks, P.C. Stair, K.R. Poeppelmeier, C.L. Marshall, Propane oxidation over Pt/SrTiO<sub>3</sub> nanocuboids, *ACS Catal.* 1 (2011) 629–635.
- [27] J.S. Yoon, Y.-S. Lim, B. Hyun Choi, H.J. Hwang, Catalytic activity of perovskite-type doped La<sub>0.08</sub>Sr<sub>0.92</sub>Ti<sub>1-x</sub>M<sub>x</sub>O<sub>3.8</sub> (M = Mn, Fe, and Co) oxides for methane oxidation, *Int. J. Hydrog. Energy* 39 (2014) 7955–7962.
- [28] S. Lowell, J. Shields, M. Thomas, M. Thommes, *Characterization of Porous Solids and Powders: Surface Area, Pore Size and Density*, Springer, 2004, 2017.
- [29] M. Thommes, et al., Physisorption of gases, with special reference to the evaluation of surface area and pore size distribution, *Pure Appl. Chem.* 87 (2015) 1051–1069.
- [30] E. Drozdz, L. Łancucki, A. Łacz, Synthesis, microstructural properties and chemical stability of 3DOM structures of Sr<sub>1-x</sub>TiO<sub>3</sub>, *J. Therm. Anal. Calorim.* 125 (2016) 1225–1231.
- [31] V. Berbenni, A. Marini, G. Bruni, Effect of mechanical activation on the preparation of SrTiO<sub>3</sub> and Sr<sub>2</sub>TiO<sub>4</sub> ceramics from the solid state system SrCO<sub>3</sub>–TiO<sub>2</sub>, *J. Alloys Compd.* 329 (2001) 230–238.
- [32] C.J. Fennie, K.M. Rabe, Structural and dielectric properties of Sr<sub>2</sub>TiO<sub>4</sub> from first principles, *Phys. Rev.* 68 (2003) 184111.
- [33] N. Guillén-Hurtado, F.E. López-Suárez, A. Bueno-López, A. García-García, Behavior of different soot combustion catalysts under NO<sub>x</sub>/O<sub>2</sub>. Importance of the catalyst–soot contact, *React. Kinet. Mech. Cat.* 111 (2014) 167–182.
- [34] Z. Liu, J.A. Anderson, Influence of reductant on the thermal stability of stored NO<sub>x</sub> in Pt/Ba/Al<sub>2</sub>O<sub>3</sub> NO<sub>x</sub> storage and reduction traps, *J. Catal.* 224 (2004) 18–27.
- [35] K.I. Hadjivianov, Identification of neutral and charged N<sub>2</sub>O<sub>y</sub> surface species by IR spectroscopy, *Catal. Rev. Sci. Eng.* 42 (2000) 71–144.
- [36] F.E. López-Suárez, S. Parres-Escalp, A. Bueno-López, M.J. Illán-Gómez, B. Ura, J. Trawczynski, Role of surface and lattice copper species in copper-containing (Mg/Sr)TiO<sub>3</sub> perovskite catalysts for soot combustion, *Appl. Catal. B* 93 (2009) 82–89.
- [37] A. Bueno-López, D. Lozano-Castelló, J.A. Anderson, NO<sub>x</sub> storage and reduction over copper-based catalysts. Part 1: Ba<sup>+</sup> + CeO<sub>2</sub> supports, *Appl. Catal. B* 198 (2016) 189–199.
- [38] T. Lesage, J. Saussey, S. Malo, M. Hervieu, C. Hedouin, G. Blanchard, M. Daturi, Operando FTIR study of NO<sub>x</sub> storage over a Pt/K/Mn/Al<sub>2</sub>O<sub>3</sub>–CeO<sub>2</sub> catalyst, *Appl. Catal. B* 72 (2007) 166–177.
- [39] L. Castoldi, I. Nova, L. Lietti, P. Forzatti, Study of the effect of Ba loading for catalytic activity of Pt–Ba/Al<sub>2</sub>O<sub>3</sub> model catalysts, *Catal. Today* 96 (2004) 43–52.
- [40] L. Lietti, P. Forzatti, I. Nova, E. Tronconi, NO<sub>x</sub> storage reduction over Pt–Ba/Al<sub>2</sub>O<sub>3</sub> catalyst, *J. Catal.* 204 (2001) 175–191.
- [41] Z. Chen, X. Wang, Y. Wang, R. Wang, Pt–Ru/Ba/Al<sub>2</sub>O<sub>3</sub>–Ce<sub>0.33</sub>Zr<sub>0.67</sub>O<sub>2</sub>: An effective catalyst for NO<sub>x</sub> storage and reduction, *J. Molec. Catal. A* 396 (2015) 8–14.